



Attosecond control of the dissociative ionization via electron localization: A comparison between D₂ and CO

P. von den Hoff^a, I. Znakovskaya^b, M.F. Kling^b, R. de Vivie-Riedle^{a,*}

^a Department für Chemie und Biochemie, Ludwig-Maximilians-Universität München, Butenandt-Strasse 11, 81377 München, Germany

^b Max-Planck-Institut für Quantenoptik, Hans-Kopfermann-Strasse 1, 85748 Garching, Germany

ARTICLE INFO

Article history:

Received 12 June 2009

Accepted 25 September 2009

Available online 2 October 2009

Keywords:

Attosecond control
Dissociative ionization
Electron localization
Electron dynamics
Carbon monoxide
D₂

ABSTRACT

Laser pulses with stable electric field waveforms establish the opportunity to achieve coherent control on attosecond timescales. A first successful example of electron localization and its control could be demonstrated for the molecules D₂⁺ and HD⁺. These molecules constitute simple model systems with only one electron and left the question open, whether electron localization in multi-electron systems can be achieved and controlled. In this context, we recently reported results where a high degree of light-waveform control over the directional emission of C⁺ and O⁺ fragments from the dissociative ionization of CO was observed [1]. Here, we compare and analyze the mechanisms leading to electron localization in the two different molecular systems D₂⁺ and CO⁺. We use our recently introduced method for multi-electron systems that allows us to describe the formation of an electronic wavepacket and to follow its evolution during the dissociation process.

© 2009 Elsevier B.V. All rights reserved.

1. Introduction

Coherent control of chemical reactions and photobiological processes has been achieved within the last decade [2,3] using pulse shapers to manipulate the light field parameters frequency, phase and polarization. Typical timescales of these processes lie in the femtosecond range. The recent accessibility of pulses with a duration of a few femtoseconds or even attoseconds [4] sparked the interest to control the dynamics of the much faster electrons. One exciting idea is to steer a chemical reaction by guiding an electronic wavepacket to the wanted position inside the molecule to form or break bonds. At least two requirements must be fulfilled, first the formation of a localizable electronic wavepacket and second its stabilization at the wanted position. An electronic wavepacket can be formed by superimposing two or more electronic states by an electric field. The sign of the applied field determines whether the positive or negative linear combination is created at the beginning of the reaction. This new paradigm of coherent control is accessible by controlling the electric field waveform $E(t) = E_0(t) \cos(\omega t + \phi)$, with envelope $E_0(t)$ and frequency ω , through the carrier envelope phase (CEP) ϕ [5].

CEP-stabilized few-cycle pulses have only recently been used to steer the electron motion in the dissociative ionization of the molecule D₂ and its isotopologues [6,7]. The asymmetric D⁺(H⁺) ion

ejection in the dissociative ionization of D₂ and HD was also theoretically studied (see e.g. [8–13] and references cited therein). After the initial ionization, these prototype systems contain a single electron. The steering of this electron originates from a CEP controlled coherent superposition of the two electronic states X²Σ_g⁺ and A²Σ_u⁺ (see Fig. 1a) that localize the electron density and finally controls the directional emission of charged and uncharged fragments upon the dissociation of the molecule.

These initial results stimulated an important question: is it possible to control the localization of electrons during reactions in more complex systems using a similar scheme? And moreover, can we identify and understand the underlying processes in the observed control? The knowledge about the processes involved is an important step towards the control of electron dynamics in molecules of chemical or biological interest. Along this line experiments on CO were performed showing encouraging results in terms of the CEP controlled electron localization during the dissociation. Control of dissociative reactions has been achieved previously by different approaches relying, e.g either on the control of the nuclear dynamics [14,15] or on the control of multipath multi-photon processes [16]. Here we focus on the reaction control through electron localization via the CEP.

The dynamics of molecules in strong laser fields typically includes ionization, recollision excitation or recombination and dissociation. In principle all these processes are steerable by the electric field waveform, and have to be considered in order to understand or even predict the outcome of a strong field experiment. While there is a wealth of work on the strong field dissociation

* Corresponding author.

E-mail addresses: matthias.kling@mpq.mpg.de (M.F. Kling), regina.de_vivie@cup.uni-muenchen.de (R. de Vivie-Riedle).

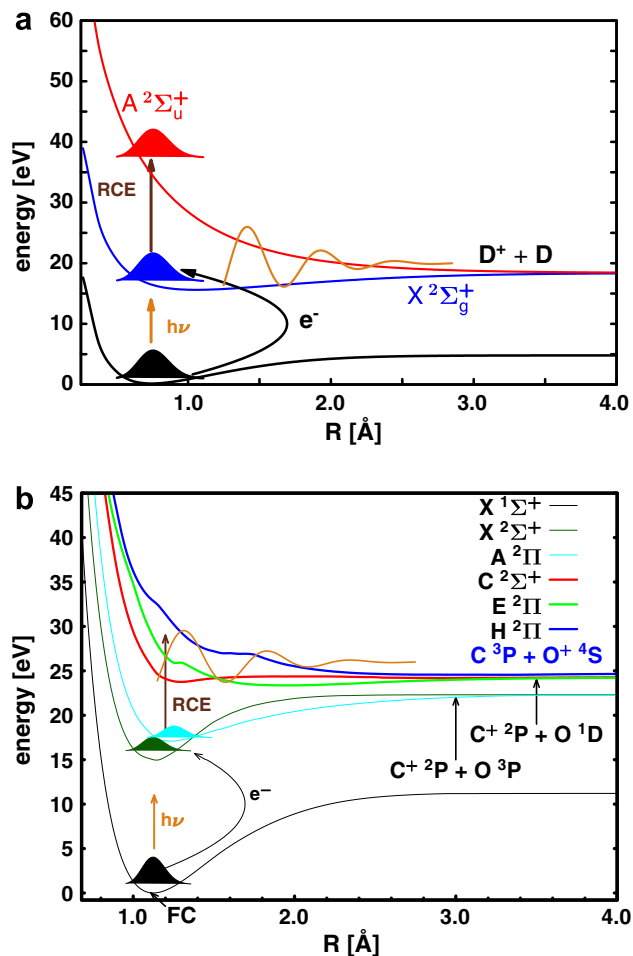


Fig. 1. (a) Potential energy surfaces (PES) of D_2, D_2^+ obtained by calculations described in the text. Pathway for the formation of D^+ ions from D_2 by dissociation of the molecular ion through ionization ($h\nu$) and recollision excitation (RCE). (b) PES of CO, CO^+ and Franck–Condon point (FC) for the ionization from neutral CO obtained by calculations described in the text. Pathway for the formation of C^+ (O^+) ions from CO by dissociation of the molecular ion through ionization ($h\nu$) and recollision excitation (RCE). For both figures it is indicated which electronic states are coupled by the remaining laser field (solid orange line). (For interpretation of the references to colour in this figure legend, the reader is referred to the web version of this article.)

tion of small molecules (see, e.g. [17] and references cited therein), only a few studies have been performed on carbon monoxide (CO) [18,19]. Very recently we reported first experimental and theoretical results on the influence of the CEP on the strong field dissociative ionization of the CO molecule [1].

In this paper we present a detailed and comparative theoretical analysis of the electron localization in the dissociative ionization of the two molecules D_2 and CO. These two molecules can be regarded as prototypes for homo- and heteronuclear systems as well as for single and multi-electron systems. We shortly refer to the experimental setup and results, as they define the initial conditions for the theoretical treatment. For the theoretical analysis, we applied our recently developed method to describe the coupled nuclear and electron dynamics simultaneously for multi-electron systems [11].

2. Experimental setup

The laser and vacuum setup used for the experiments was described in detail in [20]. The parameters for the experiments on

D_2 and CO were as follows: we generated 5 fs (D_2) and 4 fs (CO) linearly polarized, phase-stabilized pulses at 760 nm (D_2) and 740 nm (CO) with 3 kHz repetition rate. The few-cycle pulses were focused into the center of the ion optics of a velocity-map imaging (VMI) spectrometer using a spherical mirror ($f = 500$ mm (D_2)/ $f = 125$ mm (CO)). The D_2 and CO experiments with linear polarization of the laser were carried out at intensities of 1.2 and 0.8×10^{14} W/cm², respectively. Ions and electrons that were generated at the crossing point of the laser (x -axis) and an effusive atomic/molecular beam were accelerated and focused (along the z -axis) with the ion optics (see Fig. 2 consisting of a repeller, extractor and grounded time-of-flight region (from left to right in the figure) onto an MCP-phosphor screen assembly (Hamamatsu, F2226–24PX). The polarization of the laser was chosen along the y -axis, i.e. parallel to the xy -plane of the MCP detector. Images were recorded with a CCD camera. Inversion of the recorded images using an iterative inversion procedure [21] allowed reconstructing the original 3D ion momentum distributions. The pulse duration and CEP of the pulses were adjusted by insertion of fused silica into the laser beam via a pair of wedges. In the case of CO the CEP was calibrated by reference measurements in Xe and comparison to calculations based on quantitative rescattering theory according to a recently published method [22]. From the evaluation of this data the CEP is determined with an error of $\pm 0.04\pi$. For D_2 the data was recorded as a function of a relative CEP-change.

3. Experimental results

The formation of fragment ions occurs in both cases (D_2 and CO) via a two-step mechanism (schematically shown in Fig. 1a for D_2 and (b) for CO) in which initially the molecule is ionized by the laser field (Fig. 1a and b, orange arrows) and a vibrational wavepacket is created in the low-lying bound potential energy surfaces (PES) $X^2\Sigma_g^+$ for D_2 (X and A in CO^+). The dissociation is triggered by excitation to repulsive electronic states either by laser induced coupling (LC) or by recollision excitation (RCE).

The emission of fragment ions from the dissociation of D_2 and CO in intense few-cycle laser fields was monitored with VMI allowing to retrieve their full 3D-momentum distribution. Previous studies have revealed several pathways in the dissociation of D_2 and its isotopes in intense laser fields [17]. In the double ionization of these systems, two momentum-matched ions are produced that

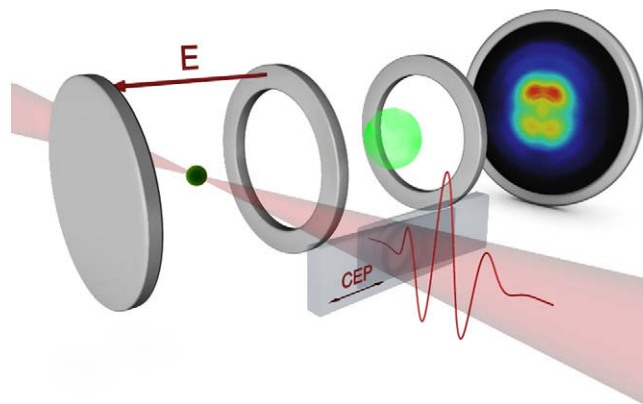


Fig. 2. Schematic of velocity-map imaging (VMI) of the directional emission of ionic fragments from the dissociative ionization of D_2 and CO with phase-stable few-cycle pulses. The CEP is shifted by the insertion of fused silica into the laser beam using a pair of wedges. Ions that are created at the crossing point of an effusive molecular jet and the focused laser beam are projected by the ion optics of the VMI, consisting of a repeller, extractor and ground plate with a grounded time-of-flight region (from left to right), onto an MCP/phosphor screen assembly. The projections (C^+ ions from CO in the schematic) are recorded by a CCD camera.

are symmetrically emitted along the molecular axis, irrespective of the evolution of the driving fields. Light-waveform control of the dissociation of D_2 thus requires to avoid double ionization pathways. The important remaining channels in the dissociative ionization of D_2 at our laser conditions are bond softening and recollision excitation [6]. Bond softening is visible by contributions to the kinetic energy spectrum of D^+ ions between 0 and 2 eV. Recollision excitation (by the electron that is emitted upon ionization of D_2) gives higher D^+ kinetic energies between 3 and 8 eV. The spectral contribution from recollision excitation vanishes with circular polarization. Fig. 3a shows the kinetic energy spectrum for the C^+ fragments from the dissociation of CO in an intense few-cycle laser field. Three main spectral peaks are visible in energy ranges of 0.15–1.5 eV, 2–2.8 eV and 3.2–3.9 eV. In the low kinetic energy range between 0.15 and 1.5 eV a distinct structure can be seen (see inset of Fig. 3a). Comparison with experiments using circular polarized (CP) light at twice the intensity as for linear polarization to achieve the same field strength, which suppresses the recollision excitation, reveal a distinct decrease of the observed C^+ ions. The resulting kinetic energy spectrum (CP) is shown in Fig. 3a. We conclude that recollision excitation is the dominant process leading to the observed fragmentation pattern while laser induced excitation from bound electronic states to dissociative states of CO^+ plays only a minor role.

No difference in the emission along the laser polarization axis (up versus down in the recorded images) is observed with a randomly varying phase. With CEP stabilization a pronounced phase dependence in the directional ion emission is found throughout the measured CEP range for D^+ ions from D_2 and C^+/O^+ ions from CO. The directional emission is represented by the angle-integrated asymmetry

$$A(W, \phi) = \frac{P_{\text{up}}(W, \phi) - P_{\text{down}}(W, \phi)}{P_{\text{up}}(W, \phi) + P_{\text{down}}(W, \phi)} \quad (1)$$

as a function of the fragment kinetic energy W and the laser phase ϕ . $P_{\text{up}}(W, \phi)$ and $P_{\text{down}}(W, \phi)$ are the measured ion yields in the up and down directions along the laser polarization axis. The ion yields were integrated over an angular range of 120° around the polarization axis over which we observed a pronounced asymmetry for both molecules (see, e.g. Fig. 4a in Ref. [7]) with almost the same amplitude. Fig. 4 shows the evolution of the asymmetry parameter $A(\phi)$ that has been obtained by integration of $A(W, \phi)$ over chosen energy intervals for D^+ ions from D_2 (panel a) and C^+ (panel b)/ O^+ (panel c)

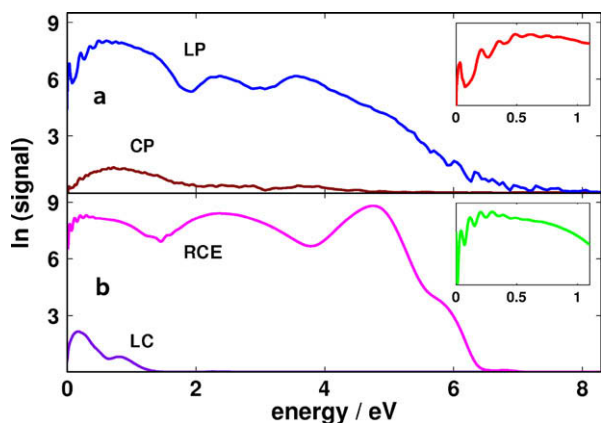


Fig. 3. (a) Experimentally observed C^+ kinetic energy spectra for CO dissociative ionization by linear (LP) and circular (CP) polarized light pulses without phase stabilization (integrated over 120°), (b) calculated C^+ kinetic energy spectrum including recollision excitation (RCE) and laser induced coupling (LC) of the bound and repulsive electronic states at the same conditions; the insets in (a) and (b) show the enlarged lower energy range for experimental and calculated spectra.

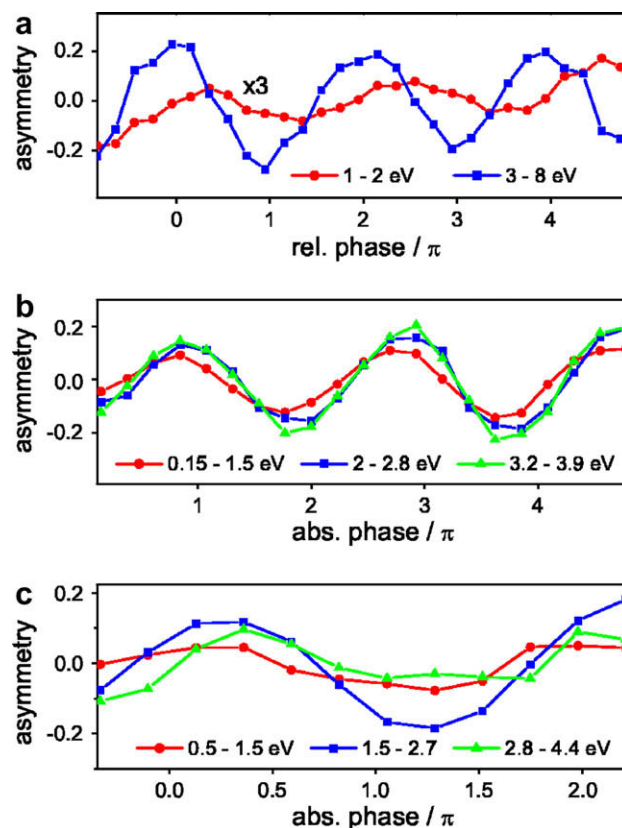


Fig. 4. Experimental asymmetry $A(\phi)$ integrated over several energy ranges (as indicated) versus the CEP for D^+ ions from D_2 (a) and C^+ ions (b)/ O^+ ions (c) from CO. For D_2 the data were recorded as a function of a relative CEP-change (rel. phase). In the case of CO the CEP was calibrated by reference measurements in Xe and comparison to calculations based on quantitative rescattering theory [22] (abs. phase).

ions from CO. In all cases the asymmetry oscillates as a function of the phase representing conditions where the direction of the ionic emission is effectively controlled. We will elaborate here further, how the mechanisms for the observed control differ for the these homo- and heteronuclear systems.

For D_2 the highest degree of control is observed for D^+ fragments, whose creation has involved recollision excitation (i.e. in the energy range between 3 and 8 eV). It has been argued in [6] that the bond softening contribution might have been affected by a temporally longer (10–20 fs) pedestal to the few-cycle pulses (of ca. 10% in intensity). Still a weak oscillation of the asymmetry in the range between 0 and 2 eV is visible and is observed to be phase-shifted with respect to the asymmetry oscillation at higher energies. Fig. 4b shows the asymmetry for C^+ ions integrated over energy ranges corresponding to the three main contributions in Fig. 3a. The observed asymmetry in the directional emission of the C^+ ions is almost equally strong throughout the whole kinetic energy spectrum with a maximum value around 0.2. Analogous to the dependence of the asymmetric emission of O^+ ions was recorded for CO, showing the same features (see Fig. 4c). Due to a 20 times weaker O^+ signal, however, the data exhibit a lower signal-to-noise ratio. Thus it is difficult to determine the phase-shift between the points, where a maximum asymmetry is found for C^+ and O^+ ions.

4. Theoretical method

A theoretical description of electron dynamics in multi-electron molecules is still a challenge. Most approaches use time-dependent

analogous of well-established quantum chemical methods. Based upon the time-dependent Hartree–Fock theory [23] and the (explicitly) time-dependent density-functional theory [24] there are many expansions to incorporate the correlation of the electrons and make use of post-Hartree–Fock methods like TD-CI [25,26], TD-MCSCF [27] and MC-TDHF [28]. In other approaches the electronic wavefunction is directly propagated using Green's function formalism [29] or in the basis of electric eigenstates [30]. While these methods describe the electronic motion very accurately, a simultaneous quantum mechanical treatment of the nuclear motion is computationally demanding. Calculations along this line has very recently been presented for bound 4-electron system LiH [31]. The group of Takatsuka [32] therefore introduced an ansatz to couple electron dynamics in the eigenstate system to classical nuclear motion.

Recently we presented a new method to treat electron and nuclear quantum dynamics simultaneously for multi-electron systems [11]. This method was tested for the control of electron localization in D_2^+ and then applied to describe the experimental results on the dissociative ionization of CO [1]. Here, we focus on a comparison of the mechanisms leading to the electron localization observed in the dissociative ionizations of D_2 and CO and the consequences for the CEP controlled asymmetry. For both prototype molecules the ionization step determines the angular distribution of the ionic fragments recorded by the VMI spectrometer (see Fig. 2). The D^+ ion distribution from D_2 is aligned along the laser polarization, while C^+ and O^+ fragments from CO show distinct maxima around 45° , 135° , 225° and 315° [1]. The angular distribution also defines the optical transitions addressable for a given laser polarization. For the heteronuclear molecule, one can expect orientational dependent ionization probabilities for phase-stabilized lasers and thus a contribution from the ionization to the total observed asymmetry [1]. Homonuclear diatomic molecules always show a symmetric angular distribution in the ionization step. The contributions from the recollision are still unknown and their calculation is currently out of scope for many electron molecules [9].

For the calculations of the asymmetry produced in the dissociation process, we follow the dominant recollision excitation pathway, assuming ionization at the electric field maximum of the strong ultrashort laser pulse and recollision of the electron 1.7 fs later (corresponding to the first recollision time [33]). Thereby the initially formed nuclear wavepacket is excited from the X (and A state in case of CO^+) to higher electronic states. Simultaneously, the electronic and nuclear wavepacket motion is launched. Important for the starting conditions of our theoretical analysis are the differences in the recollision excitation between the two molecular ions D_2^+ and CO^+ . In the case of D_2^+ the recollision excitation only populates the repulsive $A^2\Sigma_u^+$ state (see Fig. 1a). In contrast, the recollision can excite various close lying electronic states in the CO^+ molecule (see Fig. 1b). Our quantum dynamical simulations start after the recollision event. We summarize briefly our method [11] and highlight the expressions especially important for the aspired comparison. The molecular wavefunction Ψ_{mol} is set up in a product ansatz as the sum over the electronic states i involved in the subsequent laser pulse interaction:

$$\begin{aligned}\Psi_{\text{mol}}(R, r, t) &= \sum_i \varphi_i(r, t; R) \chi_i(R, t) \\ &= \sum_i \varphi_i(r, t_0; R) e^{-iE_i(R)t} \sum_j c_{ij} \xi_{ij}(R) e^{-iv_{ij}t} \\ &= \sum_i \varphi_i(r, t_0; R) \sum_j c_{ij} \xi_{ij}(R) e^{-i(E_i(R)+v_{ij})t}\end{aligned}\quad (2)$$

with χ_i the nuclear wavepackets in the i th electronic state composed of the ξ_{ij} vibrational eigenfunctions, $\varphi_i(r, t_0; R)$ the stationary

electronic wavefunction defined at time zero ($t_0 \hat{=} t = 0$), $E_i(R)$ the electronic eigenenergy, v_{ij} the relative energy of the vibrational levels, the nuclear and electronic coordinates R and r and the time t . To follow first the nuclear wavepacket motion we, multiply the time-dependent Schrödinger equation from left with $\varphi_i^*(r, t_0; R)$ and integrate over the electronic coordinate r . This leads to the usual time-dependent Schrödinger equation for the selected coupled electronic states:

$$i \frac{\partial}{\partial t} \begin{pmatrix} \chi_1 \\ \chi_2 \\ \chi_3 \\ \vdots \end{pmatrix} = \begin{pmatrix} T_{\text{nuc}} + V_1 & -\mu_{12}\epsilon(t) & -\mu_{13}\epsilon(t) & \dots \\ -\mu_{12}\epsilon(t) & T_{\text{nuc}} + V_2 & -\mu_{23}\epsilon(t) & \dots \\ -\mu_{13}\epsilon(t) & -\mu_{23}\epsilon(t) & T_{\text{nuc}} + V_3 & \dots \\ \vdots & \vdots & \vdots & \ddots \end{pmatrix} \begin{pmatrix} \chi_1 \\ \chi_2 \\ \chi_3 \\ \vdots \end{pmatrix}\quad (3)$$

with the kinetic Hamiltonian T_{nuc} , the Born–Oppenheimer potentials V_i and the dipole coupling which is treated semiclassically with the transition dipole moment μ_{ij} times the electric field $\epsilon(t)$. μ_{ij} depends on the internuclear separation and on the angle between the molecular and the laboratory frames. The transition dipole moment is a vector defined in the molecular frame. We project the total vector for a given alignment angle onto to the polarization axis defined in the laboratory frame. For the nuclear quantum dynamics we used this projection. The time-dependent Schrödinger equation for the nuclei (Eq. (3)) is solved numerically on a one-dimensional grid with the split operator scheme [34]. For the D_2 calculations we used a spatial grid with 1200 points ranging from 0.25 to 13.23 Å. The nuclear wavefunctions were propagated for 23 fs with a time step of 0.0096 fs. The CO^+ calculations were performed on a spatial grid with 1200 points ranging from 0.5 to 10.0 Å. For the coupled electron and nuclear dynamics, the nuclear wavefunctions were propagated for 24 fs with a time step of 0.0096 fs.

The derived total nuclear wavefunction $\chi_{\text{tot}} = (\chi_1, \chi_2, \chi_3, \dots)$ is a multi-dimensional vector, spanned by the coupled wavefunctions. Their square gives the probability density of the nuclei as a function of the nuclear coordinates R .

With the help of χ_{tot} the electronic density $\rho(r_1, t; R(t))$ is expressed as a function of the electronic coordinate r_1 and time t . The total molecular wavefunction is integrated over the nuclear and over the $N - 1$ electronic coordinates (with N the total number of electrons), thereby extracting explicitly the time dependence of the electronic wavefunctions:

$$\begin{aligned}\rho(r_1, t; R(t)) &= \int \Psi_{\text{mol}}^* \Psi_{\text{mol}} dR dr_2, \dots, dr_N \\ &= \sum_{i=1}^k a_i(t)^2 |\varphi_i(r_1, t_0; R(t))|^2 \\ &+ \sum_{i=1}^k \sum_{j>i}^k 2\text{Re}\{ \langle \chi_i(R, t) | \chi_j(R, t) \rangle_R \varphi_i(r_1, t_0; R(t)) \\ &\times \varphi_j(r_1, t_0; R(t)) e^{-i\Delta E_{ij}(R(t))\Delta t + i\phi(t-\Delta t)} \}\end{aligned}\quad (4)$$

where $\rho(r_1, t; R(t))$ indicates the parametric dependence of the electron density on the nuclear coordinate R , with $R(t) = \langle \chi_{\text{tot}}(R, t) | R | \chi_{\text{tot}}(R, t) \rangle$ which is the total expectation value of the internuclear distance of the nuclear wavepacket [11]. The coefficients $a_i(t) = \sqrt{\langle \chi_i(t) | \chi_i(t) \rangle_R}$ and $a_j^2(t)$ trace the population evolution of the electronic states, $\langle \chi_i(t) | \chi_j(t) \rangle_R$ is the interference term and $\Delta E_{ij}(t) = E_j(t) - E_i(t)$ the energy difference between the electronic states i and j . k is the total number of included electronic states. The electronic wavefunctions $\varphi_i(r, t_0; R(t))$ are represented as Slater determinants. At $t = 0$ they are completely real wavefunctions as calculated from quantum chemistry. They will oscillate through phase space with a velocity given by their eigenenergies.

The electron density of the electronic state i is given by $|\varphi_i(r_1, t_0; R(t))|^2 = \sum_{n=1}^m c_n^i |\zeta_n(r_1, t_0; R(t))|^2$, with c_n^i the occupation number of the molecular orbital ζ_n in the electronic state i and the sum is over all occupied orbitals. The time evolution of the electronic wavepacket is defined by the last term of Eq. (4) and is calculated by propagation in the eigenstate basis. The coupling of the fast electron to the slower nuclear dynamics enters through the time-dependent population $a_i(t)^2$, through the interference term $\langle \chi_i(t) | \chi_j(t) \rangle_R$, which weights the degree of electronic coherence $\langle \varphi_i(r_1, t_0; R(t)) | \varphi_j(r_1, t_0; R(t)) \rangle e^{-i\Delta E_{ji}(R(t))\Delta t + \phi(t-\Delta t)}$ induced in the molecular system. The phase factor $e^{-i\Delta E_{ji}(R(t))\Delta t + \phi(t-\Delta t)}$ in Eq. (4) has to be calculated recursively to retain the memory of the progressing electronic phase evolution during the propagation of the nuclear wavepackets. This is necessary as we need the absolute phase factor in Eq. (4), which is multiplied by the calculated (completely real) electronic wavefunctions at each time step of the nuclear wavepacket propagation. Here, $\phi(t - \Delta t)$ is the absolute phase of the previous time step needed for the recursive calculation. Moreover this procedure allows us to adjust the time step (Δt in Eq. (4)) to the much faster electron dynamics. We used a one-hundredth of the time step applied in the nuclear dynamics. For $E_j(t)$ we take the eigenenergy at time t at $R(t)$. This approximation is justified as the nuclear wavepackets, produced by ultrashort laser pulses, are highly localized and the energy values corresponding to the faster and slower components of the nuclear wavepackets compensate each other. Note, the time-dependence of $E_j(t)$ can lead to a change of the group velocity of the electronic wavepacket. In case non-adiabatic coupling terms are needed to describe the system dynamics, they can be included according to the method published in [35].

From Eq. (4) it is evident that two terms, the overlap of the nuclear wavepackets propagating on different potential energy surfaces and the product of the different electronic wavefunctions are important for the electronic coherence and thus for the survival of the electronic wavepacket. If one of the terms in the double sum vanish the electron dynamics collapses. These terms also play an important role in the comparison of the electron localization in both molecules. In case one of the nuclear wavepacket separates during the propagation only the part, relevant for the described dissociative process, has to be included.

Fourier-transformation of the total nuclear wavefunction after the dissociation gives the momentum spectrum of the molecular system. It can be used to calculate the momentum distribution for the individual fragments, as both nuclei are accelerated during the dissociation with the identical force but have different masses. The kinetic energy spectra for given fragments can be obtained from their momentum distribution. Thus the kinetic energy spectrum will reflect contributions from all involved electronic states with their specific dissociation dynamics.

5. Theoretical results

5.1. Nuclear dynamics and kinetic energy spectra

For our analysis, we first have to decide, which electronic states should be included in the calculation. In the case of D_2^+ this is trivial under the current laser conditions, here only two electronic states can interact through the light field. The PES for the D_2^+ electronic ground state ($X^2\Sigma_g^+$) and the repulsive $A^2\Sigma_u^+$ state have been calculated with the quantum chemistry package Molpro [36] on the CASSCF(1,2)/6-311++G** level of theory (see Fig. 1a). The D_2^+ ions are taken to be aligned along the laser polarization axis in accordance with the maxima found in the experimental ionic fragment distribution. The kinetic energy spectrum derived from the nuclear dynamics shows only one broad contribution produced by recollision excitation between 3 and 8.0 eV in good agreement with the

experimental result. The experimentally observed spectrum between 0 and 2.0 eV originates from bond softening [8,37] and is not considered in the theoretical treatment.

In case of CO^+ the choice of the electronic states is more demanding and guidance from the experiment is needed. Selection criteria are the energy distribution of the recolliding electron and the kinetic energy of the ionic fragments (e.g. C^+ ions from the dissociation of CO^+ into $C^+ + O$). The first criterium defines the upper energetic limit for the excited states participating in the dissociative ionization. The cut-off energy for this excitation for the present laser parameters is about 13 eV (3.17 U_p where U_p is the ponderomotive potential). Therefore the PES for the CO electronic ground state, the first three $^2\Sigma$ states and the first six $^2\Pi$ states for the CO^+ molecular ion (Fig. 1b) are calculated with the quantum chemistry package Molpro [36] on the CASSCF(6,12)/aug-cc-pVQZ and CASSCF(5,12)/aug-cc-pVQZ level of theory. This selection includes the highest lying σ and π electrons in the active space for the electron correlation. From the reachable excited state manifold we chose three potential curves to represent the induced dissociative dynamics resulting in the observed asymmetry and kinetic energy spectrum of the ejected ionic fragments. A further selection criterium was that all transitions among the selected states were allowed. We performed test calculations by exchanging the electronic states. From comparison with the experimental kinetic energy spectrum we could deduce that the $C^2\Sigma^+$ and $H^2\Pi$ states are needed, the C state as a weakly bound state to obtain the structure in the low kinetic energy spectrum and the H state, as the first and only reachable state leading to the $C(^3P) + O(^4S)$ channel, to allow localization of the electron density also on the C-atom (delivering O^+ fragments). The $E^2\Pi$ state is included to mimic the manifold of similar repulsive states. Exchange of this state with any other state in the reachable energetic region does not change neither the underlying mechanism nor the features of the kinetic energy spectrum. For the recollision excitation we assume a gaussian energy distribution for the returning electron performing the excitation likewise an ultrashort electric light field and start with a 55:38:7 distribution of the states involved (ordered in increasing energy). This population distribution was chosen as it delivers the experimentally observed ratio between C^+ and O^+ fragments. Whether the initial population of the excited states caused by the recollision is slightly dependent on the CEP or not is an open question, but its calculation is currently out of scope for larger molecules [9]. Multiple recollisions of the ejected electron from subsequent half-cycles are less probable under the current laser conditions and are thus neglected in the calculations [33,38].

The CO^+ ions are taken to be aligned at an angle of 45° to the laser polarization, allowing on one hand all transitions between the Σ and Π states. On the other hand the 45° orientation coincides with the angle for the maximum number of experimentally detected ionic fragments. Field-free rotation is neglected in the calculations as it takes place on a much longer timescale (approx. 8.5 ps for a full rotation of CO at its equilibrium distance). Also dynamic alignment before dissociation induced by the laser field is neglected because of the extremely short pulse duration used in the experiments on CO (4 fs).

The kinetic energy spectrum for the C^+ ions derived from the nuclear dynamics is shown in Fig. 3b and is in reasonable qualitative agreement with the experimental data supporting again the selection made for the representative states. On the basis of these results, we can explain the origin of the observed energy distribution. The low kinetic energy spectrum (0.15–1.5 eV) arises from the dynamics on the weakly bound $C^2\Sigma^+$ state and the spectrum in the range between 2.0 and 2.8 eV from the purely repulsive $E^2\Pi$ state. Both states correlate with the second dissociation channel ($C(^2P) + O(^1D)$). The high energy spectrum reflects the dynamics of the second repulsive $H^2\Pi$ state correlating with the third

reaction channel ($C(^3P) + O(^4S)$). The reason why this channel, leading to O^+ fragments, is observable in the recorded C^+ signal lies in the quantum nature of the nuclear wavefunction involved and was explained in Section 4. The structure in the low kinetic energy spectrum follows from interference effects in the nuclear wavepacket on the $C^2\Sigma^+$ state and can also be seen in the experimental spectrum. This interference appears because the recollision excitation produces a high energy wavepacket consisting of both bound and continuum vibrational states on the $C^2\Sigma^+$ surface. During the break-up of CO^+ the bound vibrational states are trapped in the potential well and interfere with the outgoing part of the wavepacket (see Fig. 5). The temporal evolution of the interference pattern can be directly connected to the vibrational levels of the $C^2\Sigma^+$ state (likewise demonstrated in Ref. [39] for D_2^+). The kinetic energy spectrum of the O^+ fragments (not shown here) reveals similar features.

The minor route of laser induced excitation from low lying bound electronic states $X^2\Sigma^+$ and $A^2\Pi$ to the dissociative states of CO^+ that was observed in the experiments using circular polarization (CP) was also included in the calculations. Fig. 3b (LC) shows the resulting kinetic energy spectrum. Only small contributions are recognizable in the kinetic energy ranges 0.15–1.5 eV and 2.0–2.5 eV (not visible within the graphical resolution of the figure).

5.2. Electron localization and asymmetry

The temporal evolution of the electronic state population during the laser pulse interaction is shown in Fig. 6a and c for both molecules. In the case of D_2^+ the nuclear dynamics starts in the $A^2\Sigma_u^+$ state prepared after the recollision excitation event. Here the nuclear dynamics is fast enough to reach the region where the energy difference between the $X^2\Sigma_g^+$ and $A^2\Sigma_u^+$ state comes into resonance with the light field. As a result, we observe a strong molecule light interaction with a large population exchange, nearly leading to a population inversion. Almost the same population transfer is found when the CEP is flipped by π (see Fig. 6a). Contrarily, in CO^+ the population of the individual states is mirrored when the CEP is flipped by π . Moreover only a weak coupling between the electronic states is achieved because the conditions for resonance are never fulfilled (see Fig. 6c).

In Fig. 6b and d we show the magnitudes derived from the electron density, which visualize the electron wavepacket motion and are connected to the experimentally observed asymmetry (see Eq. (1)). In D_2^+ we plotted the asymmetry in the electron density A

$$A = \frac{P_{up} - P_{down}}{P_{up} + P_{down}} \quad (5)$$

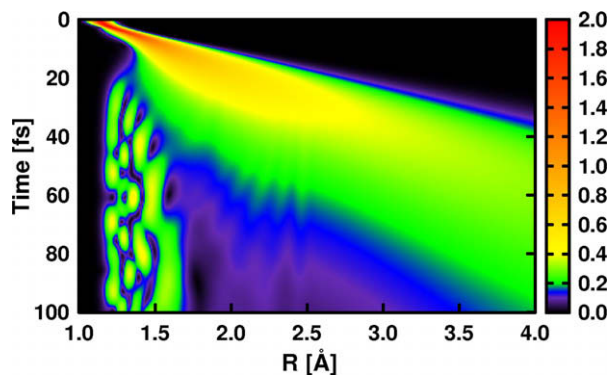


Fig. 5. Time evolution of the probability amplitude of the nuclear wavepacket in the $C^2\Sigma^+$ state of CO^+ as a function of the internuclear distance.

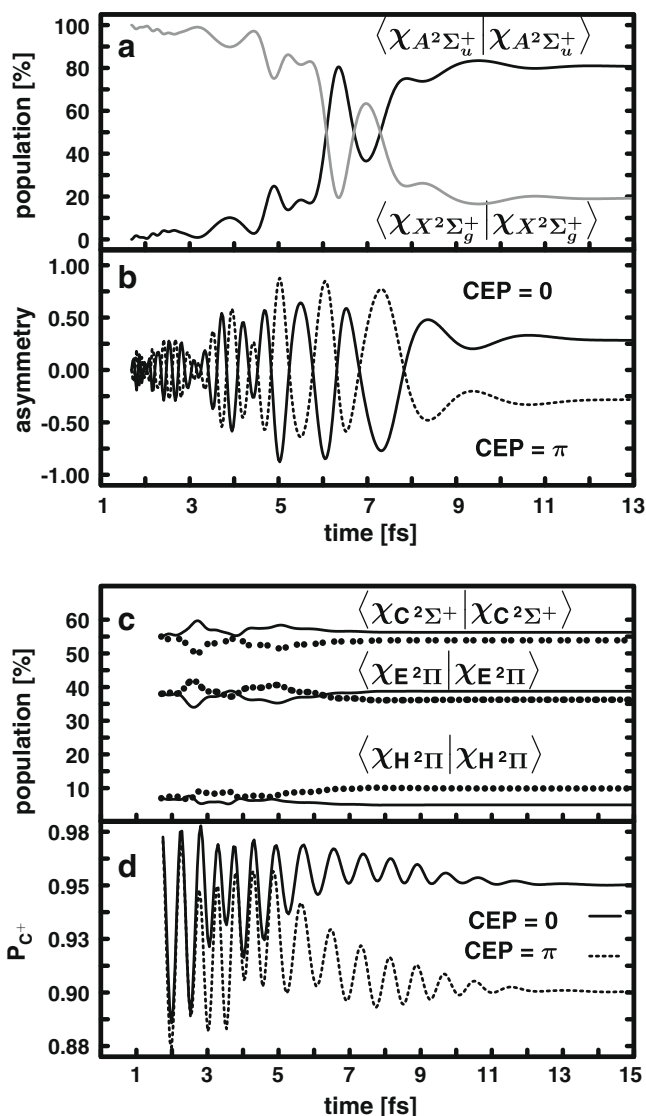


Fig. 6. (a) Time-dependent population of the $X^2\Sigma_g^+$ and $A^2\Sigma_u^+$ state of D_2^+ during the dissociation. (b) Temporal evolution of the asymmetry of D_2^+ starting from the time of recollision (solid: CEP = 0; dotted: CEP = π). (c) Time-dependent populations of the $C^2\Sigma^+$, $E^2\Pi$ and $H^2\Pi$ states of CO^+ after recollision excitation (solid: CEP = 0; dotted: CEP = π). (d) Temporal evolution of the probability measuring a C^+ fragment P_c^+ for the dissociative ionization of CO^+ after recollision (solid: CEP = 0; dotted: CEP = π).

directly connected to the experimentally measured asymmetry, with P_{up} and P_{down} the probability density to find the electron on the upper or lower D atom, respectively, given by

$$P_{up} = \int_{x_{min}}^{x_{max}} dx \int_{y_{min}}^{y_{max}} dy \int_{z_{min}}^0 dz |\varphi_{tot}(r, t_f; R(t_f))|^2 \quad (6)$$

$$P_{down} = \int_{x_{min}}^{x_{max}} dx \int_{y_{min}}^{y_{max}} dy \int_0^{z_{max}} dz |\varphi_{tot}(r, t_f; R(t_f))|^2 \quad (7)$$

The overall dynamics of the asymmetry in D_2^+ (Fig. 6b) results from a competition between the influence of the light pulse, the time evolution of the linear combination which oscillates with $\Delta E_{ij}(t)$ and the interference term of the nuclear wavefunctions, which weighs the degree of electronic coherence. During the dissociation the amplitude of the oscillation increases as the two states involved couple most efficiently. The electron dynamics stops when the two states become degenerate. By flipping the CEP by π the evolution of

the asymmetry is exactly mirrored. The maximum value for the resulting asymmetry is around 0.2 and thus close to the experiment.

In case of CO^+ the definition of the asymmetry is slightly more complex. Here the experimentally measured asymmetry arises from the ensemble of randomly oriented CO molecules. Thus P_{up} and P_{down} , respectively, are assigned to the different orientations. From both orientations C^+ and O^+ fragments can be detected and the asymmetry cannot be derived directly from the electron density of a single molecule with only one specific orientation. In our calculations we have direct access to the probability $P_{\text{C}}^+(t)$ of measuring a C^+ fragment for a given orientation. This probability is given by

$$P_{\text{C}}^+(t) = \int_{x_{\text{min}}}^{x_{\text{max}}} dx \int_{y_{\text{min}}}^{y_{\text{max}}} dy \int_{z_{\text{min}}}^0 dz \rho(r_1, t; R(t)) \quad (8)$$

where x, y and z refer to the molecular frame with z along the molecular axis and the O-Atom oriented along negative z -values. Now the CEP dependent asymmetry as observed in the experiment can be approximated by the final $P_{\text{C}}^+(t)$ values from two different orientations.

The electron dynamics reflected in $P_{\text{C}}^+(t)$ (e.g. solid curve in Fig. 6d) results like in D_2^+ , but only in the first 6 fs, from a competition between the influence of the light pulse, the time evolution of the linear combination and the interference term of the nuclear wavefunctions. As soon as the light induced population transfer between the electronic states stops (approximately after 8 fs, see Fig. 6c), the oscillation in $P_{\text{C}}^+(t)$ decreases rapidly converging after 12 fs to its final value. Responsible for the decay is the reduced overlap of the superimposed electric wavefunctions. This effect can be visualized by the molecular orbitals which discriminate the different Slater determinants and become soon located on the two different nuclei during the dissociation (see Fig. 7b). Therefore the term containing the overlap of the Slater determinants ($\phi_i(r_1, t; R)\phi_j(r_1, t; R)$) see Eq. (4) becomes zero. Consequently, the last term of Eq. (4) vanishes and with it the dynamics of the electronic linear combination. The damping of the oscillations in $P_{\text{C}}^+(t)$ reflects the decay of the initially prepared electronic wavepacket. The probability $P_{\text{C}}^+(t)$ upon the break up of the molecule is given by the final population distribution of the coupled reaction channels leading either to C^+ or O^+ fragments. This ratio is steered very precisely by the CEP of ultrashort laser pulses. A shift of the CEP by π while keeping the molecular orientation leads to a different result (dotted curve in Fig. 6d). Changing the orientation of the molecule by 180° is equal to shifting the CEP by π as the transition dipole moment changes the sign. Thus in practise, the CEP dependent asymmetry in the dissociation step can be calculated by $P_{\text{C}}^+(t)$ for two CEP values shifted by π . The maximum value for the resulting asymmetry due to the electron localization is around 0.03, but is not directly comparable to the experimental values as the ionization has significant contributions to the total asymmetry [1].

5.3. Mechanisms for electron localization

Comparison of the attosecond control mechanisms for electron localization in both molecules shows three major differences. The first one occurs already in the preparation step. In D_2^+ the superposition of the electronic states is created by the interaction with the light pulse. Thus the sign of the initial superposition is directly controlled by the CEP. Consequently, the electronic wavepackets prepared with opposite CEP values show already from the beginning exactly mirrored asymmetry values. In the case of CO^+ , the electron localization dynamics is triggered by the recollision excitation. Thus the oscillation in $P_{\text{C}}^+(t)$ for the different CEP values is prepared and proceeds almost in phase in the beginning of the dissociation and is controlled later by the laser pulse interaction. As a

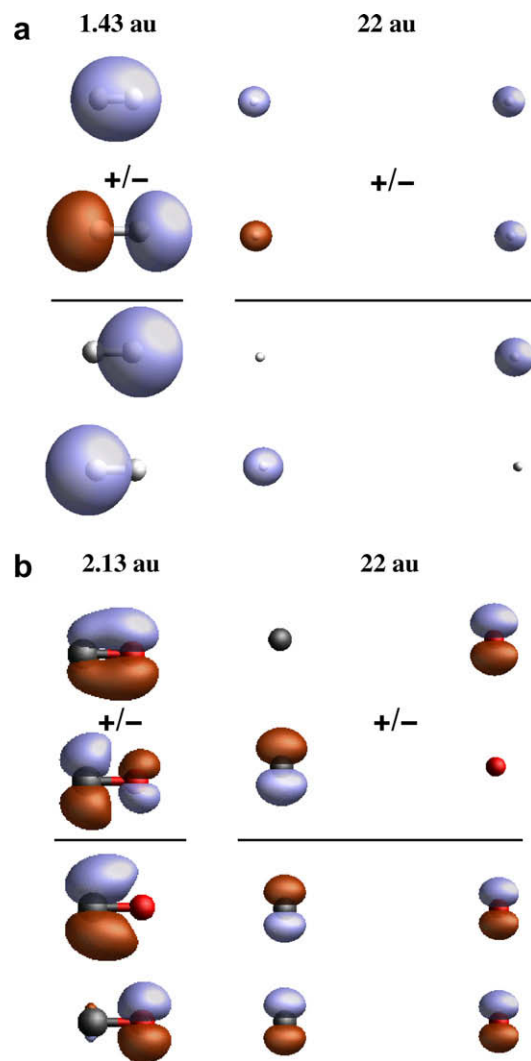


Fig. 7. (a) σ^- , σ^+ -orbitals of the D_2^+ molecule at internuclear distances 1.43 (left) and 22 au (right). The solid line separates the initial orbitals (upper half) from the calculated linear combinations of these orbitals (lower half). The positive linear combination is plotted first. For both internuclear distances the linear combinations are localized on one atomic center. (b) π_x^- , π_y^- -orbitals of the CO^+ molecule at internuclear distances 2.13 (left) and 22 au (right). The solid line separates the initial orbitals (upper half) from the calculated linear combinations of these orbitals (lower half). The positive linear combination is plotted first. For internuclear distances around the minimum geometry (left) the linear combination can localize the electron density on one atomic center. For larger distances (right) the linear combinations are delocalized.

second difference the electron localization in D_2^+ shows much larger amplitudes compared to CO^+ , because only for the lighter molecule the nuclear dynamics is fast enough to hit the resonance with the laser frequency.

The third major difference lies in the ending of the electron dynamics. In the case of the D_2^+ molecule the dynamics only stops when the two electronic states involved become degenerate and consequently the exponent in Eq. (4) becomes zero. Simultaneously, the dissociation process is completed and the degree of electron localization is determined, beside the mixing ratio of the electronic states, by the final phase of the exponential factor. For the CO^+ molecule the dynamics stops because the overlap of the electronic wavefunctions becomes zero as soon as the outer orbitals localize on one atomic center. This mechanism is shown in Fig. 7. For internuclear distances around the minimum geometry the valence molecular orbitals of both molecules are delocalized

over both centers (Fig. 7a and b left side above solid line). By forming the positive or the negative linear combination of the corresponding Slater determinants, the electron density in both cases is localized on one atom (Fig. 7a and b, left side below solid line). For larger internuclear distances the situation changes completely (Fig. 7a and b, right). In the case of the homonuclear D_2^+ the two orbitals are still delocalized over the molecule (Fig. 7a right side above solid line) and the linear combination still localizes the electron density (Fig. 7a right side below solid line). The same effect will appear for its isotopologues HD^+ and HD_2^+ as the electronic structure does not change compared to D_2^+ . For the heteronuclear CO^+ the molecular orbitals localize during the dissociation (Fig. 7b right side above solid line). Thus the electron density of the superposition state delocalizes (Fig. 7b right side below solid line). Consequently, the degree of electron localization is not determined by the phase evolution (second term of Eq. (4)) but by the populations of the electronic states which localize the electron on one or the other nucleus in their asymptotic limits (e.g. C^+ or O^+ channels). These populations are controllable by the CEP on the attosecond timescale.

6. Conclusion

For two different types of molecules, we compared the attosecond control mechanism of electron localization observed in the dissociative ionization with intense ultrashort phase-stabilized light fields. We chose the molecules D_2 and CO , which can be regarded as representatives for homo- and heteronuclear diatomics. In addition these molecules differ in the complexity of the electronic structure and most notably for both molecules experimental data were available to us [1,6]. To follow the process of electron localization during the dissociation, we applied our method for the simultaneous treatment of the coupled nuclear and electron wavepacket dynamics. Our analysis revealed significant differences in the attosecond control mechanisms. They occur already in the formation of the electronic wavepacket. In D_2^+ the electronic wavepacket is created exclusively through the light field induced coupling of only two electronic states. Thus the sign of the initial superposition is defined and controllable by the CEP. In CO^+ it is essential that the electronic wavepacket is already formed in the recollision step. Here the CEP control arises from the subsequent interaction of the laser pulse with the previously prepared electronic wavepacket and is due to the interplay of the signs of the light field and the transition dipole moments. The explanation for the differences in the preparation step can be found in the electronic structure of both molecules. In the multi-electron system many close lying electronic states exist, which are simultaneously populated by recollision excitation. We also observed differences in the electron dynamics during the dissociation. Crucial for driving the electron motion in D_2^+ is that the oscillation frequency of the electronic wavepacket comes into resonance with the laser frequency. As this never happens in the case of CO^+ the decay of the electronic wavepacket is much faster and the dominant feature. Decisive for the final degree of localization is again the electronic structure of the molecules. In D_2^+ the structure of the molecular orbitals hold the localization of the electron density in the superposition upon the break up of the molecule. This is not possible for CO^+ . Here, the electronic structure results in a delocalized electron density. For the final asymmetry we can state that for D_2^+ the phase of the superposition (exponent in Eq. (4)) imprinted by the CEP defines its final value. In the case of CO^+ the asymmetry arises from the CEP controlled population ratio between the coupled reaction channels leading either to C^+ or O^+ . It should be noted that the experimentally observed asymmetry in the case of CO is also affected by the ionization in a few-cycle phase-stable laser field

as described in [1]. With the current experimental data it is not possible to distinguish clearly between contributions from the ionization and laser-induced electron localization mechanisms in CO . Future studies are aimed into this direction. We have shown that electron localization is not restricted to one-electron systems but can be found also in multi-electron systems and understood by our theoretical calculations. Moreover, we can deduce that multiple molecular dependent pathways exist to realize electron localization. However, it will still be a great challenge to guide and stabilize an electronic wavepacket inside a given molecule to control the outcome of a reaction.

Acknowledgments

We acknowledge F. Krausz and M.J.J. Vrakking for support and fruitful discussion. We are grateful for support by the DFG via the Emmy-Noether program and the Cluster of Excellence: Munich Center for Advanced Photonics (<http://www.munich-photonics.de>).

References

- [1] I. Znakovskaya, P. von den Hoff, S. Zherebtsov, A. Wirth, O. Herrwerth, M. Vrakking, R. de Vivie-Riedle, M. Kling, Attosecond control of electron dynamics in carbon monoxide, *Phys. Rev. Lett.* 103 (2009) 103002.
- [2] P. Nuernberger, G. Vogt, T. Brixner, G. Gerber, Femtosecond quantum control of molecular dynamics in the condensed phase, *Phys. Chem. Chem. Phys.* 9 (2007) 2470.
- [3] T. Brixner, G. Gerber, Quantum control of gas-phase and liquid-phase femtochemistry, *Chem. Phys. Chem.* 4 (2003) 418.
- [4] F. Krausz, M. Ivanov, Attosecond physics, *Rev. Mod. Phys.* 81 (2009) 163.
- [5] R. Kienberger, M. Uiberacker, M.F. Kling, F. Krausz, Attosecond physics comes of age: from tracing to steering of electrons at sub-atomic scales, *J. Mod. Opt.* 54 (2007) 1985.
- [6] M.F. Kling, C. Siedschlag, A.J. Verhoef, J.I. Khan, M. Schultze, T. Uphues, Y. Ni, M. Uiberacker, M. Drescher, F. Krausz, M.J.J. Vrakking, Control of electron localization in molecular dissociation, *Science* 312 (2006) 246–248.
- [7] M.F. Kling, C. Siedschlag, I. Znakovskaya, A.J. Verhoef, S. Zherebtsov, F. Krausz, M. Lezius, M.J.J. Vrakking, Strong-field control of electron localization during molecular dissociation, *Mol. Phys.* 106 (2008) 455.
- [8] V. Roudnev, B. Esry, I. Ben-Itzhak, Controlling HD^+ and H_2^+ dissociation with the carrier-envelope phase difference of an intense ultrashort laser pulse, *Phys. Rev. Lett.* 93 (16) (2004) 163601.
- [9] S. Gräfe, M.Y. Ivanov, Effective fields in laser-driven electron recollision and charge localization, *Phys. Rev. Lett.* 99 (2007) 163603.
- [10] X.M. Tong, C.D. Lin, Dynamics of light-field control of molecular dissociation at the few-cycle limit, *Phys. Rev. Lett.* 98 (2007) 123002.
- [11] D. Geppert, P. von den Hoff, R. de Vivie-Riedle, Electron dynamics in molecules: a new combination of nuclear quantum dynamics and electronic structure theory, *J. Phys. B: At. Mol. Opt. Phys.* 41 (2008) 074006.
- [12] A.D. Bandrauk, S. Chelkowski, H.S. Nguyen, Attosecond localization of electrons in molecules, *Int. J. Quant. Chem.* 100 (6) (2004) 834–844.
- [13] A.D. Bandrauk, S. Chelkowski, P.B. Corkum, J. Manz, G.L. Yudin, Attosecond photoionization of a coherent superposition of bound and dissociative molecular states: effect of nuclear motion, *J. Phys. B: At. Mol. Opt. Phys.* 42 (2009) 134001.
- [14] H. Lippert, J. Manz, M. Oppel, G.K. Paramonov, W. Radloff, H.-H. Ritze, V. Stert, Control of breaking strong versus weak bonds of $BaFCH_3$ by femtosecond IR + VIS laser pulses: theory and experiment, *Phys. Chem. Chem. Phys.* 6 (2004) 4283–4295.
- [15] B. Amstrup, N.E. Henriksen, Control of HOD photodissociation dynamics via bond-selective infrared multiphoton excitation and a femtosecond ultraviolet laser pulses, *J. Chem. Phys.* 97 (1992) 8285.
- [16] I. Thanopoulos, M. Shapiro, Enhanced selectivity and yield in multichannel photodissociation reactions: application to CH_3I , *J. Chem. Phys.* 125 (2006) 133314.
- [17] J.H. Posthumus, The dynamics of small molecules in intense laser fields, *Rep. Prog. Phys.* 67 (2004) 623.
- [18] C. Guo, Holding molecular dications together in strong laser fields, *Phys. Rev. A* 73 (2006) 041401.
- [19] A.S. Alnaser, C.M. Maharjan, X.M. Tong, B. Ulrich, P. Ranitovic, B. Shan, Z. Chang, C.D. Lin, C.L. Cocke, I.V. Litvinyuk, Effects of orbital symmetries in dissociative ionisation of molecules by few-cycle laser pulses, *Phys. Rev. A* 71 (2005) 031403.
- [20] M. Schultze, E. Goulielmakis, M. Uiberacker, M. Hofstetter, J. Kim, D. Kim, F. Krausz, U. Kleineberg, Powerful 170-attosecond XUV pulses generated with few-cycle laser pulses and broadband multilayer optics, *New J. Phys.* 9 (2007) 243.
- [21] M.J.J. Vrakking, An iterative procedure for the inversion of two-dimensional ion/photoelectron imaging experiments, *Rev. Sci. Instr.* 72 (2001) 4084.

- [22] S. Micheau, Z. Chen, A.T. Le, J. Rauschenberger, M.F. Kling, C.D. Lin, Accurate retrieval of target structures and laser parameters of few-cycle pulses from photoelectron momentum spectra, *Phys. Rev. Lett.* 102 (2009) 073001.
- [23] K.C. Kulander, Time-dependent Hartree–Fock theory of multiphoton ionization: helium, *Phys. Rev. A* 36 (6) (1987) 2726–2738.
- [24] E. Runge, E.K.U. Gross, Density-functional theory for time-dependent systems, *Phys. Rev. Lett.* 52 (12) (1984) 997.
- [25] T. Klamroth, Laser-driven electron transfer through metal–insulator–metal contacts: time-dependent configuration interaction singles calculations for a Helium model, *Phys. Rev. B* 68 (2003) 245421.
- [26] N. Rohringer, A. Gordon, R. Santra, Configuration-interaction-based time-dependent orbital approach for ab initio treatment of electronic dynamics in a strong optical laser field, *Phys. Rev. A* 74 (2006) 043420.
- [27] T. Kato, H. Kono, Time-dependent multiconfiguration theory for electronic dynamics of molecules in an intense laser field, *Chem. Phys. Lett.* 392 (2004) 533.
- [28] J. Zanghellini, M. Kitzler, T. Brabec, A. Scrinzi, Testing the multi-configuration time-dependent Hartree Fock method, *J. Phys. B: At. Mol. Opt. Phys.* 37 (2004) 763.
- [29] A.I. Kuleff, J. Breidbach, L.S. Cederbaum, Multielectron wave-packet propagation: general theory and application, *J. Chem. Phys.* 123 (2005) 044111.
- [30] I. Barth, J. Manz, Y. Shigeta, K. Yagi, Unidirectional electronic ring current driven by a few cycle circularly polarized laser pulse: quantum model simulations for Mg–Porphyrin, *J. Am. Chem. Soc.* 128 (2006) 7043–7049.
- [31] M. Nest, The multi-configuration electron-nuclear dynamics method, *Chem. Phys. Lett.* 472 (2009) 171.
- [32] K. Yagi, K. Takatsuka, Nonadiabatic chemical dynamics in an intense laser field: electronic wave packet coupled with classical nuclear motions, *J. Chem. Phys.* 123 (2005) 224103.
- [33] H. Niikura, F. Légaré, R. Hasbani, A.D. Bandrauk, M.Y. Ivanov, D.M. Villeneuve, P.B. Corkum, Sub-laser-cycle electron pulses for probing molecular dynamics, *Nature* 417 (2002) 917.
- [34] C. Leforestier, R.H. Bisseling, C. Cerjan, M.D. Feit, R. Friesner, A. Guldberg, A. Hammerich, G. Jolicard, W. Karrlein, H.-D. Meyer, N. Lipkin, O. Roncero, R. Kosloff, A comparison of different propagation schemes for the time dependent Schrödinger equation, *J. Comp. Phys.* 94 (1991) 59–80.
- [35] L.S. Cederbaum, Born-oppenheimer approximation and beyond for time-dependent electron processes, *J. Chem. Phys.* 128 (2008) 124101.
- [36] H.-J. Werner, P.J. Knowles, R. Lindh, F.R. Manby, M. Schütz, et al., *Molpro*, Version 2006.1, A Package of Ab Initio Programs, 2006.
- [37] V. Roudnev, B.D. Esry, HD⁺ in a short strong laser pulse: practical consideration of the observability of carrier-envelope phase effects, *Phys. Rev. A* 76 (2007) 023403.
- [38] A.S. Alnaser, X.M. Tong, T. Osipov, S. Voss, C.M. Maharjan, P. Ranitovic, B. Ulrich, B. Shan, Z. Chang, C.D. Lin, C.L. Cocke, Routes to control of H₂ coulomb explosion in few-cycle laser pulses, *Phys. Rev. Lett.* 93 (2004) 183202.
- [39] U. Thumm, T. Niederhausen, B. Feuerstein, Time-series analysis of vibrational nuclear wave-packet dynamics in D₂⁺, *Phys. Rev. A* 77 (2008) 063401.